

THE ASTROPHYSICAL JOURNAL, 265:15–34, 1983 December 1
 © 1983. The American Astronomical Society. All rights reserved. Printed in U.S.A.

THE AGE AND COMPOSITION OF THE LMC RED GLOBULAR CLUSTER NGC 2121

PHILLIP FLOWER
 Clemson University

DOUGLAS GEISLER, PAUL HODGE,¹ AND EDWARD OLSZEWSKI¹
 University of Washington

AND

ROBERT SCHOMMER
 Rutgers University

Received 1983 February 10; accepted 1983 May 11

ABSTRACT

A color-magnitude diagram for the Large Magellanic Cloud red globular cluster NGC 2121 to $V = 21$ shows a conspicuous main sequence and a well-populated giant region. The main sequence turnoff morphology indicates an age of only ~ 0.4 billion years, and the faintest giants, when fitted to a set of evolutionary models calculated for this purpose, give a similar result. A value of $[Fe/H]$ of -1.3 ± 0.4 is obtained from the colors and magnitudes on the giant branch.

Subject headings: clusters: globular — galaxies: Magellanic Clouds — stars: abundances — stars: evolution

I. INTRODUCTION

This paper continues a series of studies of rich star clusters in the Magellanic Clouds (see summary in Hodge 1981a). The purpose of these studies is to use $C-M$ (color-magnitude) diagrams of the clusters to explore both the properties of the clusters (ages, abundances, structure, and masses) and the properties of advanced stages of stellar evolution that cannot be explored observationally in our Galaxy because of the lack of variety in the physical properties of such populous clusters.

NGC 2121 was chosen as a prime target for this work because of its apparent large age and because it is relatively open in structure, allowing photometry to be carried out even in the central regions. Its red integrated color ($B-V = 0.85$, $U-B = 0.25$, van den Bergh 1981) led Gascoigne and Kron (1952) to include it in their list of probable globular clusters, and its uncalibrated $C-M$ diagram morphology also suggested great age (Hodge 1960). Danziger's (1973) 11-color photometry led him to classify it as a globular cluster intermediate in type between M10 and NGC 6356. Hodge and Wright (1963) discovered two Cepheids in NGC 2121 (as well as noting a third Cepheid, HV 12656, near to the cluster but probably too far to be a possible member). Although their light curves are similar to those of globular cluster Cepheids, they are too bright for the Population II $P-L$ relation. Demers (1973) studied them further, concluding that variable No. 1 ($P = 5.7$) is a classical Cepheid in color and light curve. Variable No. 2

($P = 2.2$, and closer to the cluster center) was too crowded for Demers to measure its color.

Convincing evidence that NGC 2121 is not a true globular cluster came from the uncalibrated $C-M$ diagram of Hesser, Hartwick, and Ugarte (1976), who classified it as "young," and from the four-color photometry of Searle, Wilkinson, and Bagnuolo (1980), which placed it in their Class VI (next-to-the-oldest of their classes), which indicates an age in the range of 0.7–9 billion years (Hodge 1983). Lloyd Evans (1980) identified six very red stars in NGC 2121, five of which were measured in the near infrared (JHK) by Mould and Aaronson (1982), who identified LE6 as a "photometric" carbon star. On this basis, they quote an upper limit to the age of the cluster of 4×10^9 yr.

Other work on NGC 2121 has included Cohen's (1982) spectroscopic study that indicated an abundance of $[Z/Z_{\odot}] = -0.95 \pm 0.4$, based on two stars, and Rabin's (1982) spectroscopic result of $[Fe/H] \sim -1.3$ and age $\sim 5-10 \times 10^9$ yr. Also published are discussions of the cluster's ellipticity, which Geisler and Hodge (1980) found to be $\epsilon = 0.32$, making it one of the most elongated of the LMC's bright clusters. Frenk and Fall (1982), however, estimated ϵ to be only 0.18.

II. OBSERVATIONS

The observational data for this program were obtained at the Cerro Tololo Inter-American Observatory and the Las Campanas Observatory in 1979 and 1980. Plates were obtained with the LCO 2.5 meter and the CTIO 4 m telescopes (Table 1), all exposed with an auxiliary wedge (Pickering 1891; Racine 1969) to form secondary images. Deep plates were taken with the 2.5 m telescope, while the 4 m CTIO plates were

¹ Visiting Astronomer, Cerro Tololo Inter-American Observatory, which is supported by the National Science Foundation under contract AST 78-27879.

of very short exposure, taken to allow study of the inner part of the cluster. *B* plates of 47 Tucanae were taken to calibrate the difference in magnitude between primary and secondary images using Hartwick and Hesser's (1977) photoelectric sequence. The secondary images showed neither a different structure nor a departure from a constant relationship between magnitude or color and Δm , the difference in magnitude between secondary and primary images, as sometimes occurs (Blanco 1982). For the 2.5 m plates, we derived $\Delta m = 6.58 \pm 0.03$ (standard error) for 20 stars, and for the 4 m plates we obtained $\Delta m = 6.88 \pm 0.09$ for 18 stars.

Photoelectric standards (Fig. 1 and Table 2) were set up in the area adjacent to NGC 2121, covering the range $V = 9.24$ to 17.03 and $B - V = +0.12$ to $+1.41$. The 33 stars were measured with the CTIO 1.5 m, 0.9 m, and 0.6 m telescopes and the LCO 0.9 m in 1978, 1979, 1980, and 1981. In all cases standard magnitudes and colors were obtained by direct comparison to equatorial *UBV* standards, after determining extinction for each night in the standard way. One of the sequence stars, our star N, had been observed photoelectrically by Demers (1973), who quotes values for both V and $B - V$ that differ from ours by only 0.02 mag. With the auxiliary prism, the standards were extended to the effective plate limits, which on the 2.5 m plates occur at $V \sim 21.2$, $B \sim 21.7$. We did not attempt to measure images fainter than this because of severe background effects due to the faint, partially resolved LMC stellar background.

III. DATA REDUCTIONS

The photographs of NGC 2121 were reduced in two ways. The brighter stars in the central area of the cluster were scanned on the LCO plates with the KPNO PDS, with reductions carried out with the KPNO RICHFLD photometry program developed and described by Tody (1980). A 1024 square pixel raster with $0''.2$ square pixels was used, covering about $3.5'$ on the plates. In addition, small rasters around calibration stars were scanned, although these proved of limited usefulness, since the images were usually saturated on the plates. Each LCO plate had a continuous density wedge exposed on a blank portion of the plate; the

TABLE 1
PLATES OF NGC 2121

Plate Number	Observatory	Date (1979)	Exposure (minutes)	Color
627	LCO	Jan 2	45	<i>B</i>
628	LCO	Jan 2	30	<i>B</i>
635	LCO	Jan 4	40	<i>B</i>
636	LCO	Jan 4	50	<i>V</i>
637	LCO	Jan 4	45	<i>V</i>
638	LCO	Jan 4	40	<i>V</i>
4372	CTIO	Sep 26	5	<i>B</i>
4373	CTIO	Sep 26	5	<i>B</i>
4376	CTIO	Sep 26	5	<i>V</i>
4379	CTIO	Sep 26	5	<i>V</i>

TABLE 2
PHOTOELECTRIC SEQUENCE

Star	<i>V</i>	\pm	$B - V$	\pm	$U - B$	\pm	<i>n</i>
A	12.67	0.03	0.82	0.01	0.43	...	3
B	14.02	0.02	0.58	0.02	3
E	14.57	0.01	0.71	0.02	2
F	14.80	0.02	0.71	0.05	2
G	14.38	0.05	0.83	0.05	3
H	12.40	0.04	0.61	0.01	0.19	...	3
I	13.78	0.04	0.76	0.04	2
J	13.14	0.02	0.67	0.01	0.19	...	3
K	11.60	0.03	0.61	0.01	0.16	...	4
L	10.73	0.03	0.57	0.01	0.09	0.01	6
M	14.84	0.03	1.13	0.06	6
N	13.89	...	0.89	1
Q	13.14	...	0.79	1
R	11.51	0.02	0.46	0.01	0.05	0.01	2
T	14.89	0.04	0.12	0.04	7
V	15.38	...	1.03	1
W	16.38	...	0.66	1
X	16.46	...	0.81	1
Z	17.03	...	0.86	1
AA	9.89	...	0.59	1
BB	11.92	0.02	1.02	0.01	5
CC	13.04	0.02	0.56	0.03	5
1	10.91	0.01	1.41	0.01	2
2	9.24	...	0.87	1
3	12.36	...	0.51	1
4	11.26	...	0.47	1
5	13.94	...	0.51	1
7	13.36	...	1.17	1
8	14.71	0.01	0.99	0.03	2
9	15.56	0.03	0.66	0.01	2
10	14.45	...	0.23	1
11	16.40	...	0.47	1
12	16.35	...	0.92	1

run of density with position for this wedge provided the density-to-intensity calibration, and the rasters were converted to intensity units. A set of six uncrowded stars in the cluster field were combined to form the mean stellar profile for each plate (the point spread function, psf). Approximately 150 program stars were identified, and a χ^2 minimization procedure was used to determine a scaling ratio (intensity) and background value (sky plus integrated cluster background) by fitting the psf to each image. For the worst cases, interactive removal of contamination was necessary. The scale in both V and B of the derived magnitudes was found to differ significantly from that of the photometric system of the standard stars and so they were adjusted to agree. We believe that the intensity calibration of the plates is probably the cause of this discrepancy.

For these stars, plus approximately 350 more (Fig. 2), an iris astrophotometer was used on both the KPNO and the LCO plates. The cluster was divided into an inner region of radius $32''$ and an outer annulus of radius $54''$. Although the cluster itself has a rather low central concentration, the background stellar density from the main body of the Large Cloud causes crowding problems at the fainter magnitudes, and thus many of the fainter images were contaminated to some degree. The photometric indices for the stars measured

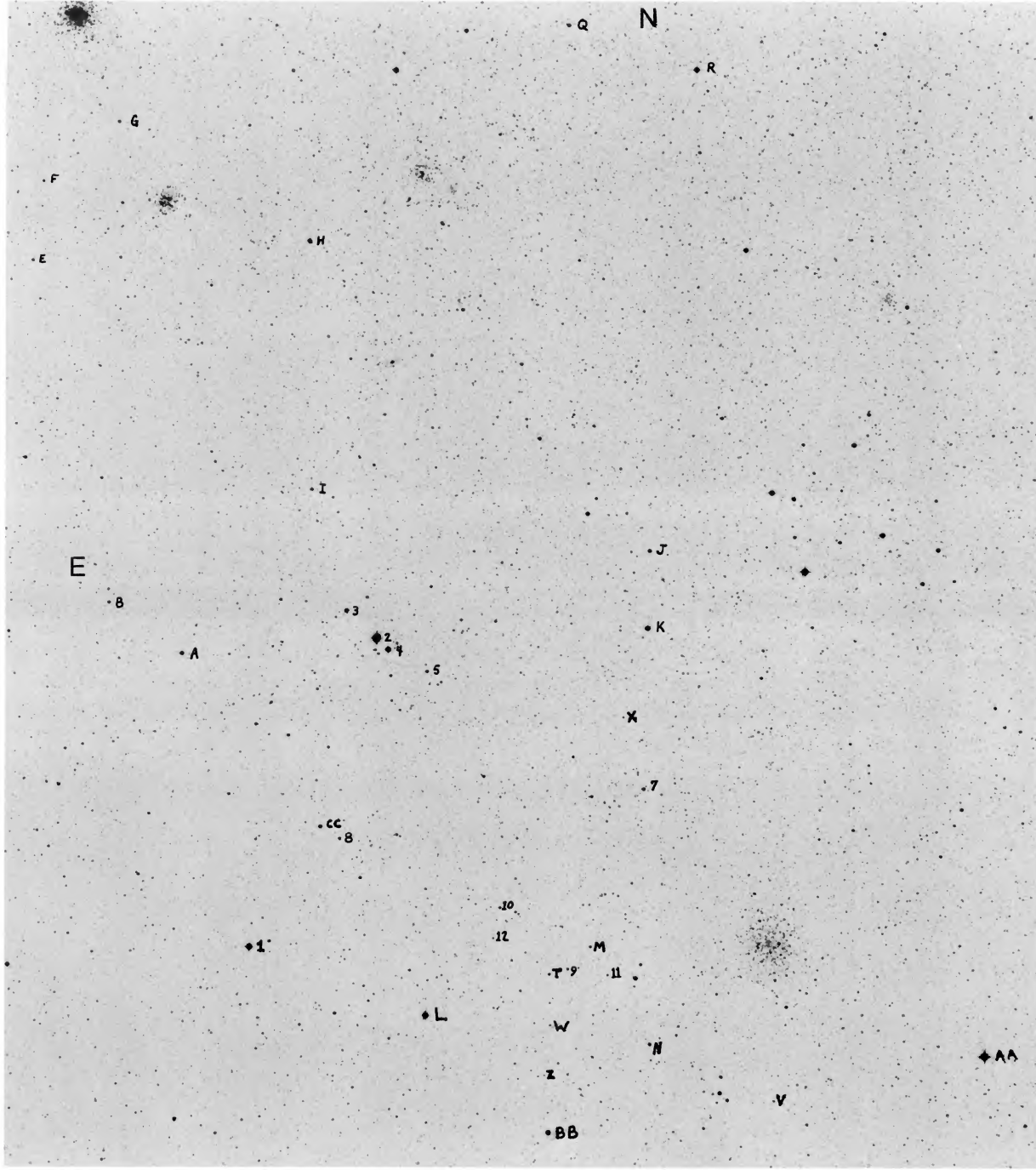


FIG. 1.—The location of the photoelectric sequence stars. The three Cepheids are also identified. From a V 2.5 m plate.

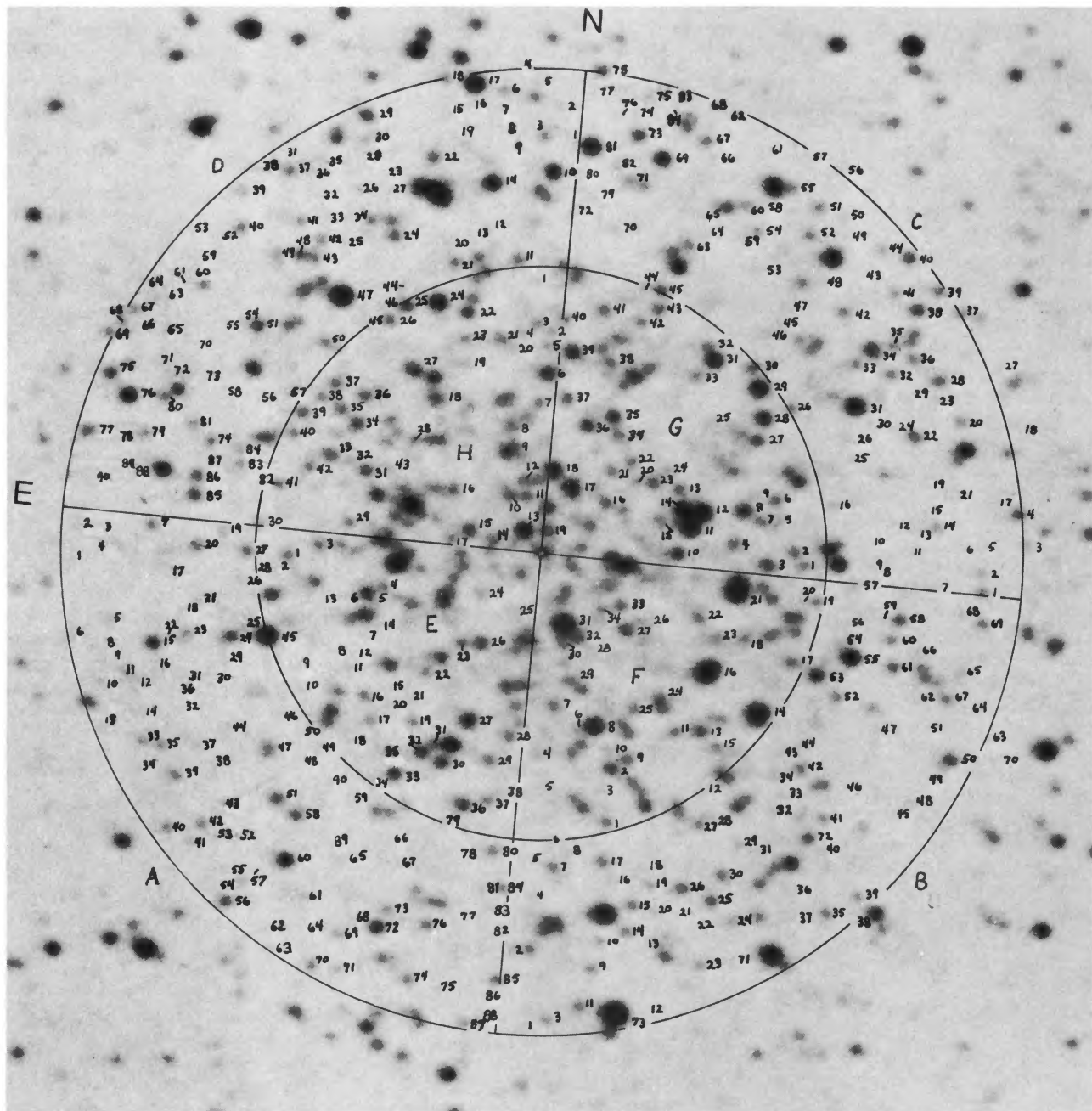


FIG. 2.—Stars measured in NGC 2121. From a 2.5 m telescope V plate.

on each plate were transformed to the photoelectric magnitude scale by fitting, in a least squares manner, a fourth order polynomial to the standard star data. Color coefficients to correct the photographic system to the photoelectric UBV system were determined in this minimization procedure. These color coefficients are determined by the equations:

$$\begin{aligned} V_{pg} &= V_{pe} + k_V(B - V)_{pe}, \\ B_{pg} &= B_{pe} + k_B(B - V)_{pe}. \end{aligned}$$

The values of k_V and k_B depend upon filter, emulsion, telescope, and exposure. The value of k_V ranged between -0.04 and 0.04 for both the 2.5 m and 4 m ; k_B varied from 0.15 to 0.20 for the 2.5 m plates and was -0.05 for the 4 m plates. The mean residual (photographically determined magnitude minus photoelectric magnitude) from all plates was 0.09 mag. We suspect, from its consistent systematic deviation in the calibration curves, that photoelectric standard Z (our faintest) should be ~ 0.3 mag fainter in both B and V .

The individual magnitudes for each star from the five plate pairs, from both the PDS and astrophotometer measures, were then combined and the average values of V , $B - V$, their standard errors, and the number of measures (plates) are given in Table 3, and plotted in Figure 3.

Crowding and background contamination are noticeable even for the brighter giants, and these effects increase with magnitude. In the outer annulus, colors and magnitudes of stars brighter than 20^{th} V magnitude are uncertain by ± 0.07 mag on average, while in the inner region this increases to ± 0.09 mag. For the stars with $V > 20$, typical errors are ± 0.1 mag in V , and ± 0.15 mag in $B - V$ for both regions. Evidently, photometric errors combined with crowding and background effects are so severe for stars fainter than $V \sim 19.5$ that the underlying cluster main sequence is smeared out to redder colors. Previous experimentation with astrophotometric techniques (e.g., Flower *et al.* 1980) has yielded similar errors in these crowded regions, and these effects probably represent a fundamental limitation of this data reduction technique. Nevertheless, these measurements are sufficiently accurate to delineate the main features of the cluster $C-M$ diagram and to provide reasonable estimates of age and metallicity from the giants and turnoff stars.

An arrow in Figure 3 indicates the position of the "photometric" carbon star LE6, which is not detectable on the blue plates and has a magnitude of 18.65 on the V plates, with an implied $B - V > 3.0$. In the BV plane, the star is quite a bit fainter than the giant branch tip because of its large bolometric correction, which Mould and Aaronson (1982) calculate to be -5.30 . It is intrinsically both brighter and redder than the other red giant tip stars identified by Lloyd Evans (1980).

IV. THE CEPHEIDS

Of the three variables in the NGC 2121 vicinity described by Hodge and Wright (1963), only V2 is

within the cluster boundaries, as defined by our chosen outline (Fig. 2) and as tabulated by Demers (1973, Table 1). It is crowded on our plates and impossible to measure with the astrophotometer. However, Demers's (1973) careful study provided a reliable mean V magnitude of $\langle V \rangle = 16.12$, which we have combined with Hodge and Wright's (1963) somewhat less certain value for $\langle B \rangle$ to derive a color of $\langle B \rangle - \langle V \rangle = +0.69$. The position of the Cepheid is shown in Figure 3, which shows it to lie near the top of the giant branch in luminosity. It is clearly not on the evolutionary track that fits the bulk of the cluster stars (see § VIII). It is either not a member, along with V1 which is even brighter, or it is a star crossing the instability strip in some unexpected post-giant phase (e.g., Flower 1982; Böhm-Vitense, Borutzki, and Harris 1982). The field $C-M$ diagram (§ VI) has several main sequence stars bright enough to be progenitors of a Cepheid this bright. However, if both V1 and V2 are field stars, then we must conclude that the general Harvard surveys of variables in the LMC must be very incomplete, on the order of only 20–25% efficient (see additional statistical arguments favoring this view in Hodge and Wright 1966).

V. THE REDDENING

We have estimated the reddening for NGC 2121 in three ways. First, we compared the UBV colors for the six photoelectric standards for which U magnitudes were available with the unreddened two-color diagram for luminosity class V stars. The best fit was for a reddening of $E_{B-V} = 0.05 \pm 0.03$, assuming a galactic-like reddening law such that $E_{U-B} = 0.73E_{B-V}$. This is the foreground galactic reddening, as all six stars are clearly main sequence dwarfs in our Galaxy. Second, we noted that Lucke (1974) measured the reddening in Association 117/118, which is the nearest association to NGC 2121 for which he quotes reddening. It is not very close to the cluster, but it does similarly lie near the SE end of the LMC bar. Assuming the dust content to be the same, we conclude that for NGC 2121, $E_{B-V} = 0.25$, which implies 0.20 mag of reddening within this part of the LMC. It also should be noted that for the clusters NGC 2058 and NGC 2065, also in this portion of the LMC, the reddenings' average is 0.18 (Flower 1982). Our third method has been to fit the main sequence of our $C-M$ diagrams to an unreddened age-zero main sequence. This is crude, both because of the known large uncertainties in the colors of our faintest stars and because of the inevitable contamination of the observed main sequence by evolved stars to the right and above the age-zero main sequence. Our best estimates based on the field $C-M$ diagram main sequence (see § VI) and the outer cluster main sequence, both for $V \sim 19.5$, are, respectively, $E_{B-V} = 0.20$ and 0.19 . From these five estimates, we conclude that the total reddening for NGC 2121 is $E_{B-V} = +0.20$, with an estimated uncertainty of ± 0.10 . We note, therefore, that the very red integrated colors of NGC 2121 (van den Bergh 1981; in $B - V$ it is the reddest, save one, of all LMC clusters) may be

TABLE 3
COLORS AND MAGNITUDES OF CLUSTER STARS

STAR	V	SE(V)	B-V	SE(B-V)	N	STAR	V	SE(V)	B-V	SE(B-V)	N
A 2	20.59	0.21	0.55	0.25	2	A80	18.68	0.04	0.94	0.08	3
A 3	20.29	0.05	0.50	0.09	2	A81	20.10	0.07	0.58	0.02	3
A 4	20.53	0.15	0.92	0.35	2	A82	20.41	0.03	0.95	0.18	2
A 5	19.80	0.08	0.30	0.05	3	A83	20.39	0.14	0.79	0.08	2
A 6	19.75	0.06	0.88	0.19	3	A84	18.84	0.03	1.09	0.07	3
A 7	18.69	0.05	0.95	0.06	3	A85	18.63	0.06	1.06	0.05	3
A 9	20.37	0.04	0.57	0.20	2	A87	19.07	0.08	0.93	0.15	3
A10	19.88	0.00	0.25	0.06	3	A88	20.13	0.04	0.61	0.14	2
A11	19.97	0.09	0.36	0.03	3	A89	20.39	--	0.85	--	1
A12	20.31	--	0.63	--	1	A90	20.13	--	0.84	--	1
A14	20.32	--	1.04	--	1	B 1	20.03	0.03	0.86	0.16	3
A15	17.99	0.05	0.02	0.07	5	B 2	19.83	0.14	1.02	0.12	3
A16	20.10	0.34	0.06	0.24	2	B 3	19.02	0.03	0.85	0.08	3
A17	20.82	--	0.44	--	1	B 4	20.03	0.06	0.52	0.12	3
A18	20.49	0.14	0.65	0.09	2	B 5	20.28	--	0.68	--	1
A19	19.26	0.11	0.50	0.04	3	B 6	19.91	--	0.67	--	1
A20	18.54	0.05	1.07	0.12	3	B 7	18.63	0.04	1.01	0.10	3
A21	20.19	0.02	0.60	0.15	3	B 8	19.85	0.02	0.61	0.11	3
A22	19.85	0.04	0.79	0.06	3	B 9	18.85	0.05	0.29	0.03	3
A23	18.89	0.09	1.15	0.15	3	B10	19.19	0.05	1.15	0.12	3
A24	18.12	0.04	0.27	0.02	3	B11	18.61	0.06	1.06	0.08	3
A25	19.75	0.16	0.28	0.08	2	B12	20.69	--	0.78	--	1
A26	19.88	0.06	1.08	0.13	3	B13	20.81	--	0.54	--	1
A27	18.50	0.08	1.12	0.05	3	B14	18.71	0.09	1.18	0.05	3
A28	20.34	--	0.88	--	1	B15	18.57	0.07	0.32	0.03	3
A29	20.33	0.04	0.56	0.04	3	B16	19.62	0.12	0.88	0.06	3
A30	20.15	0.11	1.09	0.19	2	B17	18.54	0.07	0.95	0.05	3
A32	20.53	0.17	0.86	0.36	2	B18	19.91	0.02	0.63	0.04	3
A33	19.43	0.09	1.11	0.16	3	B19	19.13	0.04	1.05	0.10	3
A34	20.39	0.00	0.69	0.17	2	B20	19.71	0.03	0.96	0.06	3
A35	19.11	0.02	0.92	0.03	3	B22	20.56	--	0.39	--	1
A37	20.19	0.08	0.39	0.11	3	B23	19.10	0.01	1.27	0.15	3
A38	20.00	--	0.76	--	1	B24	19.20	0.02	0.87	0.06	3
A39	18.64	0.07	1.12	0.07	3	B25	18.26	0.07	1.23	0.03	3
A40	18.70	0.11	1.40	0.12	3	B26	18.29	0.04	0.22	0.02	4
A41	19.58	0.06	1.07	0.11	3	B27	18.69	0.04	1.09	0.08	3
A42	18.77	0.08	1.09	0.05	3	B28	19.80	0.03	0.68	0.05	3
A43	21.11	--	0.63	--	1	B29	19.63	0.03	0.09	0.02	3
A44	20.13	0.06	0.17	0.01	3	B30	18.56	0.07	0.96	0.10	3
A45	16.60	0.02	1.60	0.06	3	B31	19.90	0.02	0.55	0.10	3
A46	20.40	--	0.36	--	1	B32	20.10	0.07	0.69	0.14	3
A47	18.45	0.05	0.04	0.10	4	B33	20.29	0.20	0.95	0.11	2
A49	20.04	0.03	0.85	0.13	3	B34	19.86	0.03	0.45	0.06	3
A50	20.93	--	0.38	--	1	B35	18.64	0.07	1.26	0.05	3
A51	18.20	0.06	1.06	0.05	3	B36	20.44	--	0.51	--	1
A52	19.53	0.07	1.22	0.12	3	B37	20.36	0.13	0.98	0.05	2
A53	20.08	0.11	0.79	0.20	2	B38	20.44	0.00	1.00	0.37	2
A54	20.29	--	0.95	--	1	B39	19.03	0.03	1.26	0.02	3
A55	21.05	--	0.40	--	1	B40	20.01	0.08	0.97	0.02	3
A56	18.24	0.06	1.09	0.03	3	B41	18.85	0.08	1.20	0.03	3
A57	20.38	--	1.32	--	1	B42	18.55	0.07	1.08	0.11	3
A58	18.26	0.07	1.22	0.04	3	B43	20.24	0.04	0.84	0.18	2
A59	20.45	0.06	0.79	0.20	2	B44	20.47	--	0.63	--	1
A60	17.55	0.02	1.28	0.04	3	B45	20.33	0.10	0.14	0.07	3
A61	19.76	0.02	0.21	0.10	3	B46	20.43	--	0.82	--	1
A62	20.47	0.06	0.15	0.02	2	B47	19.92	0.08	1.19	0.20	2
A63	20.01	0.05	0.34	0.06	3	B48	19.75	0.09	0.53	0.12	3
A64	20.37	--	0.77	--	1	B49	20.37	--	0.89	--	1
A65	19.77	0.08	0.27	0.03	3	B50	18.14	0.04	0.21	0.05	5
A66	20.42	0.00	0.67	0.12	2	B51	20.45	--	1.33	--	1
A67	20.47	--	0.65	--	1	B52	18.75	0.03	0.97	0.04	3
A68	20.06	0.07	0.70	0.17	2	B53	17.81	0.03	1.27	0.11	3
A69	19.13	0.06	0.30	0.03	3	B54	19.25	0.10	0.30	0.19	3
A70	18.80	0.11	1.20	0.12	3	B55	17.13	0.02	1.40	0.05	5
A71	19.51	0.08	0.19	0.12	3	B56	20.07	0.08	0.68	0.14	2
A72	17.86	0.05	1.13	0.04	3	B57	19.85	0.03	0.67	0.13	2
A73	18.96	0.03	0.29	0.04	3	B58	18.19	0.08	1.35	0.02	3
A74	18.71	0.07	1.05	0.13	3	B59	20.09	0.10	0.74	0.06	3
A75	20.41	0.03	0.43	0.06	3	B60	18.60	0.11	1.08	0.07	3
A76	18.58	0.07	1.07	0.07	3	B61	18.28	0.12	1.17	0.07	2
A78	20.67	--	0.77	--	1	B62	20.05	--	0.83	--	1
A79	19.94	0.07	0.37	0.04	3	B63	20.57	--	0.79	--	1

TABLE 3—Continued

STAR	V	SE(V)	B-V	SE(B-V)	N	STAR	V	SE(V)	B-V	SE(B-V)	N
B64	20.29	--	0.94	--	1	C67	18.57	0.10	1.13	0.11	3
B65	19.74	0.05	0.75	0.06	3	C68	20.41	0.06	1.02	0.18	3
B66	19.66	0.07	0.87	0.07	3	C69	17.58	0.02	1.23	0.03	3
B67	18.80	0.06	1.06	0.10	3	C70	19.78	0.04	0.13	0.00	3
B68	20.26	0.09	0.65	0.13	3	C71	18.90	0.03	0.97	0.04	3
B69	18.62	0.10	1.06	0.07	3	C72	20.02	--	0.60	--	1
B70	20.66	--	0.64	--	1	C73	18.08	0.09	1.26	0.10	3
B71	20.31	0.22	0.81	0.21	2	C74	20.15	--	0.60	--	1
B72	18.22	0.07	1.02	0.03	3	C75	19.82	0.14	0.29	0.10	3
B73	15.68	0.01	1.14	0.03	5	C76	20.39	0.22	0.96	0.48	2
C 1	18.96	0.09	1.07	0.13	3	C77	20.76	--	0.64	--	1
C 2	19.58	0.10	0.29	0.13	3	C78	18.24	0.05	0.35	0.10	5
C 3	19.56	0.05	0.20	0.04	3	C79	20.48	--	0.72	--	1
C 4	18.27	0.10	1.39	0.06	3	C80	19.88	0.09	0.61	0.03	3
C 5	20.94	--	0.41	--	1	C81	17.16	0.04	0.94	0.08	3
C 7	20.30	0.18	0.96	0.36	2	C82	19.58	0.03	0.72	0.11	2
C 8	20.37	--	0.84	--	1	C83	20.61	--	0.65	--	1
C 9	20.01	0.09	0.91	0.04	2	C84	20.38	--	0.79	--	1
C10	20.88	--	0.56	--	1	D 1	20.30	0.08	1.08	0.11	2
C11	21.11	--	0.57	--	1	D 2	20.12	0.07	0.95	0.11	3
C12	20.70	0.24	0.78	0.38	2	D 3	20.28	0.06	0.86	0.17	3
C13	20.07	0.02	1.02	0.25	2	D 4	20.55	--	0.62	--	1
C14	18.95	0.04	1.16	0.09	3	D 5	20.15	0.11	0.80	0.07	2
C15	20.81	0.34	0.90	0.49	2	D 6	18.93	0.04	1.17	0.08	3
C16	19.70	0.04	0.46	0.02	3	D 7	20.53	0.02	0.69	0.09	2
C17	20.40	0.04	0.63	0.03	2	D 8	20.48	--	1.18	--	1
C18	20.34	0.00	0.69	0.07	2	D 9	20.65	--	0.78	--	1
C19	20.38	--	0.80	--	1	D10	17.49	0.01	1.16	0.04	3
C20	18.96	0.04	1.08	0.09	3	D11	18.48	0.06	1.04	0.07	3
C21	20.17	--	0.90	--	1	D12	20.00	0.08	0.57	0.05	3
C22	18.31	0.06	0.93	0.07	3	D13	20.27	0.08	0.72	0.01	?
C23	19.89	0.13	1.19	0.13	3	D14	17.29	0.03	1.20	0.09	5
C24	20.30	0.01	0.58	0.08	2	D15	20.26	0.07	0.80	0.03	2
C25	20.58	--	0.58	--	1	D16	20.23	0.00	1.08	0.09	2
C26	19.53	0.10	0.53	0.09	3	D17	16.94	0.03	1.42	0.05	5
C27	20.87	0.29	0.42	0.16	2	D18	18.79	0.12	1.31	0.13	3
C28	18.40	0.05	0.98	0.10	3	D19	20.53	--	0.93	--	1
C29	20.28	--	0.79	--	1	D20	19.91	0.06	0.66	0.10	2
C30	20.26	0.11	0.87	0.19	3	D21	18.59	0.07	1.13	0.03	3
C31	17.02	0.03	1.29	0.05	5	D22	18.28	0.08	1.08	0.07	3
C32	18.65	0.02	1.04	0.12	3	D23	20.57	--	0.82	--	1
C33	18.80	0.05	1.21	0.11	3	D24	18.26	0.05	1.21	0.07	3
C34	17.77	0.01	1.06	0.00	3	D25	20.47	--	1.00	--	1
C35	18.72	0.05	1.20	0.10	3	D26	20.30	0.04	0.80	0.12	2
C36	18.67	0.02	0.33	0.04	3	D27	20.05	0.12	0.93	0.18	2
C37	18.96	0.02	1.02	0.01	3	D28	20.18	0.08	1.03	0.11	2
C38	18.05	0.09	1.36	0.09	3	D29	17.99	0.07	1.24	0.05	3
C39	18.59	0.06	1.11	0.05	3	D30	19.17	0.08	1.22	0.09	3
C40	18.19	0.08	1.39	0.05	3	D31	20.42	--	0.84	--	1
C41	18.90	0.05	1.12	0.07	3	D32	20.16	0.20	0.36	0.02	2
C42	18.73	0.06	1.02	0.10	3	D33	20.24	0.21	1.09	0.25	2
C44	19.25	0.06	1.20	0.09	3	D34	20.35	0.01	1.09	0.20	2
C45	19.95	0.18	0.76	0.05	2	D35	19.86	--	1.12	--	1
C46	19.84	0.11	0.44	0.07	2	D36	20.19	0.10	0.53	0.04	2
C47	19.97	0.05	0.31	0.03	3	D37	18.42	0.07	1.20	0.04	3
C48	20.18	0.10	0.76	0.06	3	D38	20.26	0.11	0.63	0.13	3
C49	20.45	0.14	0.78	0.08	2	D39	19.26	0.08	0.48	0.03	3
C50	20.22	0.11	0.58	0.05	3	D40	18.64	0.07	1.21	0.06	3
C51	18.67	0.07	1.04	0.04	3	D41	18.88	0.08	1.19	0.08	3
C52	18.70	0.07	1.11	0.05	3	D42	18.79	0.04	1.06	0.03	3
C53	19.90	0.04	0.99	0.12	3	D43	18.41	0.08	1.03	0.14	2
C54	19.06	0.03	1.19	0.09	3	D44	20.24	--	1.23	--	1
C55	18.45	0.01	1.12	0.10	3	D45	20.13	0.05	0.61	0.06	3
C56	20.24	0.16	0.53	0.23	2	D47	16.45	0.03	1.47	0.08	5
C58	20.40	--	0.78	--	1	D48	18.34	0.09	1.01	0.09	2
C59	20.07	0.01	0.66	0.10	2	D49	19.14	0.01	0.31	0.05	3
C60	18.89	0.07	1.06	0.12	3	D50	18.66	0.08	1.11	0.07	3
C61	20.31	--	1.26	--	1	D51	18.00	0.07	1.18	0.03	3
C63	18.57	0.05	1.05	0.09	3	D53	20.43	0.29	0.92	0.42	2
C64	20.44	--	0.66	--	1	D54	20.08	--	1.35	--	1
C65	20.12	0.05	0.68	0.09	3	D55	20.94	--	0.97	--	1
C66	20.42	--	0.63	--	1	D56	20.62	--	0.91	--	1

TABLE 3—Continued

STAR	V	SE(V)	B-V	SE(B-V)	N	STAR	V	SE(V)	B-V	SE(B-V)	N
D57	20.18	0.10	0.73	0.07	3	F 6	19.37	0.24	0.45	0.30	3
D58	20.64	--	0.82	--	1	F 7	18.53	0.01	0.95	0.09	3
D61	20.41	--	0.39	--	1	F 8	17.01	0.04	1.42	0.03	3
D62	18.72	0.05	1.05	0.05	3	F 9	18.30	0.03	0.88	0.07	3
D63	20.36	0.09	0.54	0.01	2	F10	19.54	0.13	0.31	0.17	3
D64	20.22	0.03	0.98	0.17	3	F11	18.58	0.02	1.14	0.09	3
D66	20.48	0.01	1.06	0.11	2	F12	20.29	0.18	0.72	0.28	2
D67	19.03	0.04	0.38	0.03	3	F13	18.03	0.07	1.06	0.12	3
D68	19.08	0.04	1.06	0.05	3	F14	16.31	0.03	1.55	0.07	5
D69	18.58	0.10	1.15	0.07	3	F15	18.60	0.14	1.04	0.17	2
D71	20.36	0.04	0.71	0.16	3	F16	16.24	0.06	1.11	0.14	5
D72	19.89	0.05	1.08	0.04	3	F17	18.45	0.03	0.91	0.19	3
D73	20.56	0.09	0.78	0.21	3	F18	18.58	0.05	1.01	0.12	3
D74	18.77	0.04	1.10	0.05	3	F19	18.69	0.07	1.20	0.08	3
D75	18.14	0.07	1.23	0.03	3	F20	19.96	0.12	0.46	0.15	2
D76	17.46	0.02	0.59	0.05	5	F21	16.00	0.09	1.75	0.05	3
D77	18.36	0.06	1.06	0.09	3	F22	18.45	0.07	0.96	0.07	3
D78	20.36	0.22	0.92	0.31	2	F23	18.76	0.01	0.49	0.18	3
D79	18.94	0.06	0.44	0.09	3	F24	17.89	--	0.89	--	1
D80	18.61	0.03	1.12	0.13	3	F25	18.52	0.04	0.92	0.12	3
D81	18.85	0.09	1.12	0.10	3	F26	19.06	0.04	0.12	0.15	3
D82	20.32	0.01	0.39	0.11	2	F27	17.91	0.02	0.79	0.13	3
D83	18.98	0.06	0.92	0.10	3	F28	19.71	0.14	0.28	0.14	3
D84	19.34	0.03	0.94	0.09	3	F29	18.38	0.00	0.68	0.10	2
D85	18.05	0.07	1.20	0.05	3	F30	18.04	0.11	0.26	0.08	2
D86	18.30	0.07	0.94	0.01	3	F31	16.09	0.06	1.52	0.09	3
D87	20.51	0.08	0.57	0.18	2	F32	17.91	0.05	0.83	0.12	3
D88	20.19	0.04	0.39	0.20	2	F33	18.26	0.03	0.95	0.08	3
D89	20.78	--	0.66	--	1	F34	18.82	0.03	0.45	0.21	2
D90	20.29	0.03	0.42	0.12	3	G 1	18.54	0.07	1.13	0.17	3
D91	20.71	0.20	0.76	0.30	2	G 2	18.38	0.06	0.52	0.07	3
E 1	18.52	0.10	1.19	0.10	3	G 3	18.00	0.04	0.87	0.05	3
E 2	20.27	0.07	1.28	0.22	2	G 4	18.29	0.04	0.63	0.20	3
E 3	18.59	0.04	1.11	0.13	3	G 5	19.27	0.03	0.46	0.11	3
E 4	18.60	0.01	0.23	0.08	3	G 6	18.45	0.05	0.99	0.07	3
E 5	17.84	0.03	0.95	0.05	3	G 7	18.43	0.06	1.06	0.08	3
E 6	20.34	0.16	0.76	0.01	2	G 8	17.68	0.02	0.84	0.12	3
E 7	20.22	0.11	0.32	0.12	3	G 9	19.53	0.10	0.49	0.08	3
E 9	20.10	0.05	1.10	0.08	2	G10	17.93	0.01	0.91	0.03	2
E10	20.22	0.21	1.10	0.33	2	G11	16.86	--	0.25	--	1
E11	19.96	0.08	0.20	0.14	3	G12	16.71	--	1.24	--	1
E12	20.34	0.15	1.04	0.01	2	G13	18.30	0.05	1.19	0.07	3
E13	20.53	--	0.70	--	1	G14	16.72	--	0.64	--	1
E14	19.91	--	0.53	--	1	G15	18.63	0.05	0.37	0.12	3
E15	20.19	0.04	0.85	0.10	3	G16	18.30	0.05	0.76	0.12	3
E16	18.71	0.07	1.16	0.14	3	G17	17.19	0.07	0.85	0.13	3
E17	18.94	0.04	0.90	0.04	3	G18	17.24	0.05	0.88	0.20	3
E18	20.17	0.05	0.61	0.00	2	G19	17.89	0.03	0.49	0.22	3
E19	18.81	0.05	1.16	0.10	3	G20	18.97	0.07	0.11	0.10	3
E20	20.18	0.15	0.59	0.01	2	G21	18.49	0.06	0.98	0.21	3
E21	20.19	0.04	0.71	0.19	2	G22	18.54	0.03	0.86	0.13	3
E22	18.69	0.06	0.96	0.06	3	G23	18.29	0.01	0.47	0.26	3
E23	18.47	0.05	1.19	0.10	3	G24	19.29	0.08	0.35	0.13	3
E24	19.22	0.03	0.47	0.10	3	G25	19.83	0.07	0.63	0.08	3
E25	19.79	0.13	0.23	0.03	2	G26	18.72	0.03	1.20	0.11	3
E26	17.98	0.05	1.16	0.08	3	G27	18.07	0.03	0.85	0.06	2
E27	17.58	0.03	0.93	0.08	4	G28	17.55	0.03	1.20	0.03	3
E28	18.56	0.05	0.95	0.17	3	G29	17.08	0.04	1.17	0.04	3
E29	18.55	0.03	1.05	0.06	3	G30	18.30	0.02	1.05	0.08	3
E30	17.92	0.02	1.09	0.05	3	G31	17.27	0.02	1.02	0.02	4
E31	18.26	0.02	1.11	0.14	3	G32	18.24	0.02	1.13	0.09	3
E32	17.92	0.03	1.12	0.04	3	G33	18.74	0.05	0.93	0.05	3
E33	17.93	0.05	1.28	0.03	3	G34	18.35	0.01	0.88	0.15	3
E34	19.87	0.12	0.50	0.11	3	G35	17.77	0.02	0.76	0.04	3
E35	20.18	0.09	0.48	0.18	3	G36	17.88	0.02	1.07	0.06	3
E36	17.95	0.03	0.11	0.03	5	G37	18.34	0.06	0.91	0.11	3
E37	18.75	0.02	0.88	0.12	3	G38	18.31	0.03	0.75	0.11	3
E38	19.63	0.11	0.94	0.09	2	G39	17.72	0.01	1.12	0.04	3
F 1	18.56	0.03	0.33	0.01	3	G40	18.69	0.01	0.99	0.05	3
F 2	18.02	0.03	0.97	0.05	3	G41	18.35	0.08	0.99	0.10	3
F 3	20.08	0.16	0.39	0.36	2	G42	18.61	0.09	1.19	0.05	3
F 4	19.63	0.09	0.61	0.15	3	G43	18.42	0.05	0.90	0.11	3

TABLE 3—Continued

STAR	V	SE(V)	B-V	SE(B-V)	N	STAR	V	SE(V)	B-V	SE(B-V)	N
G44	19.61	0.10	0.32	0.16	3	H20	19.43	0.10	0.15	0.00	2
G45	18.26	0.07	1.20	0.06	3	H21	18.46	0.10	0.76	0.15	2
G46	17.61	0.10	0.34	0.12	2	H22	17.95	0.04	0.94	0.03	2
G47	18.49	0.06	0.98	0.15	3	H23	18.74	0.05	1.11	0.09	3
G48	18.18	0.05	0.77	0.09	2	H24	17.23	0.03	1.27	0.04	3
H 1	20.06	0.07	0.59	0.06	3	H25	17.99	0.05	1.11	0.06	3
H 2	19.09	0.02	0.81	0.08	3	H26	18.45	0.06	1.02	0.06	3
H 3	18.86	0.01	1.31	0.14	3	H27	17.86	0.01	0.89	0.03	3
H 4	19.65	0.13	0.44	0.17	3	H28	18.73	0.04	1.10	0.12	3
H 5	18.96	0.01	0.78	0.09	3	H29	18.72	0.03	1.08	0.11	3
H 6	17.70	0.02	0.47	0.16	3	H30	19.12	0.07	0.93	0.11	3
H 7	18.55	0.07	1.15	0.08	3	H31	18.09	0.06	1.08	0.06	3
H 8	18.38	0.01	0.03	0.20	2	H32	19.10	0.06	0.41	0.10	3
H 9	17.63	0.07	0.63	0.30	2	H33	18.11	0.04	0.93	0.10	3
H10	18.27	--	0.49	--	1	H34	18.04	0.04	0.90	0.11	3
H11	18.20	0.05	0.86	0.25	2	H35	18.34	0.06	0.80	0.06	3
H12	18.20	--	0.94	--	1	H36	18.24	0.05	0.85	0.09	3
H13	17.23	0.07	1.00	0.09	3	H37	18.41	0.02	1.04	0.12	3
H14	18.27	0.03	0.79	0.11	2	H38	18.74	0.01	1.02	0.07	3
H15	17.98	0.03	0.78	0.06	3	H39	18.34	0.06	1.08	0.08	3
H16	18.36	0.02	0.68	0.18	3	H40	18.57	0.02	1.03	0.06	3
H17	18.60	0.02	0.94	0.13	3	H41	18.68	0.08	1.19	0.08	3
H18	17.94	0.05	0.53	0.11	3	H42	18.61	0.06	1.06	0.13	3
H19	19.47	0.02	0.49	0.12	3	H43	19.46	0.08	0.77	0.21	3

largely due to this high value for E_{B-V} . Corrected colors place it closer to the other intermediate age objects.

VI. THE COMPARISON FIELD

Because the main sequence of NGC 2121 is of critical importance in establishing its nature and its age, we have been especially careful to account as accurately as

possible for the contamination of the C-M diagram by field (foreground and background) stars. Figure 4 shows an area of the LMC adjacent to NGC 2121 (4.5 NNW) for which we measured colors and magnitudes of stars in an area of approximately 2.5 (arcmin)². Table 4 gives the average V , $B-V$, and their standard errors, from iris photometry of the two deepest plate pairs. Figure 5 shows the field C-M diagram. The

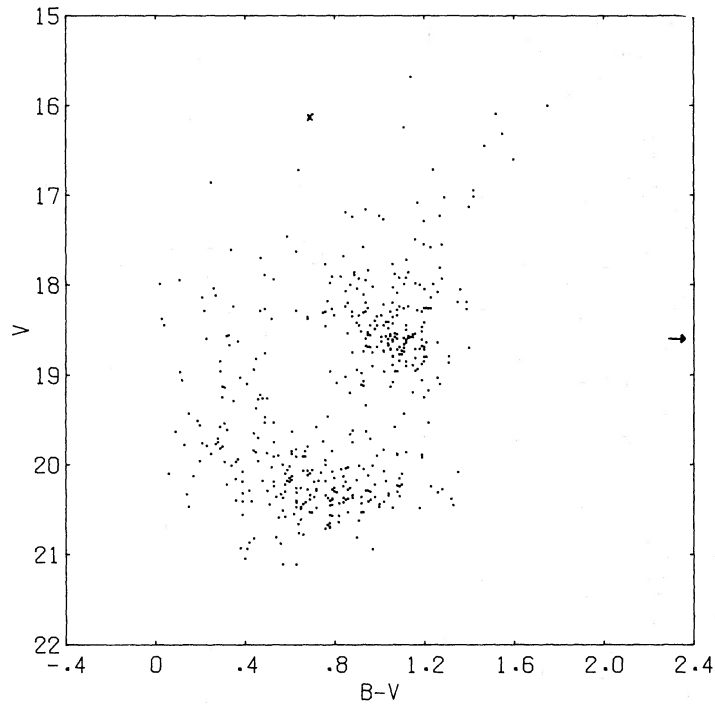


FIG. 3.—The complete C-M diagram for NGC 2121, including foreground and background stars. The arrow indicates the V level of the carbon star, and the X indicates mean position for the Cepheid V2.

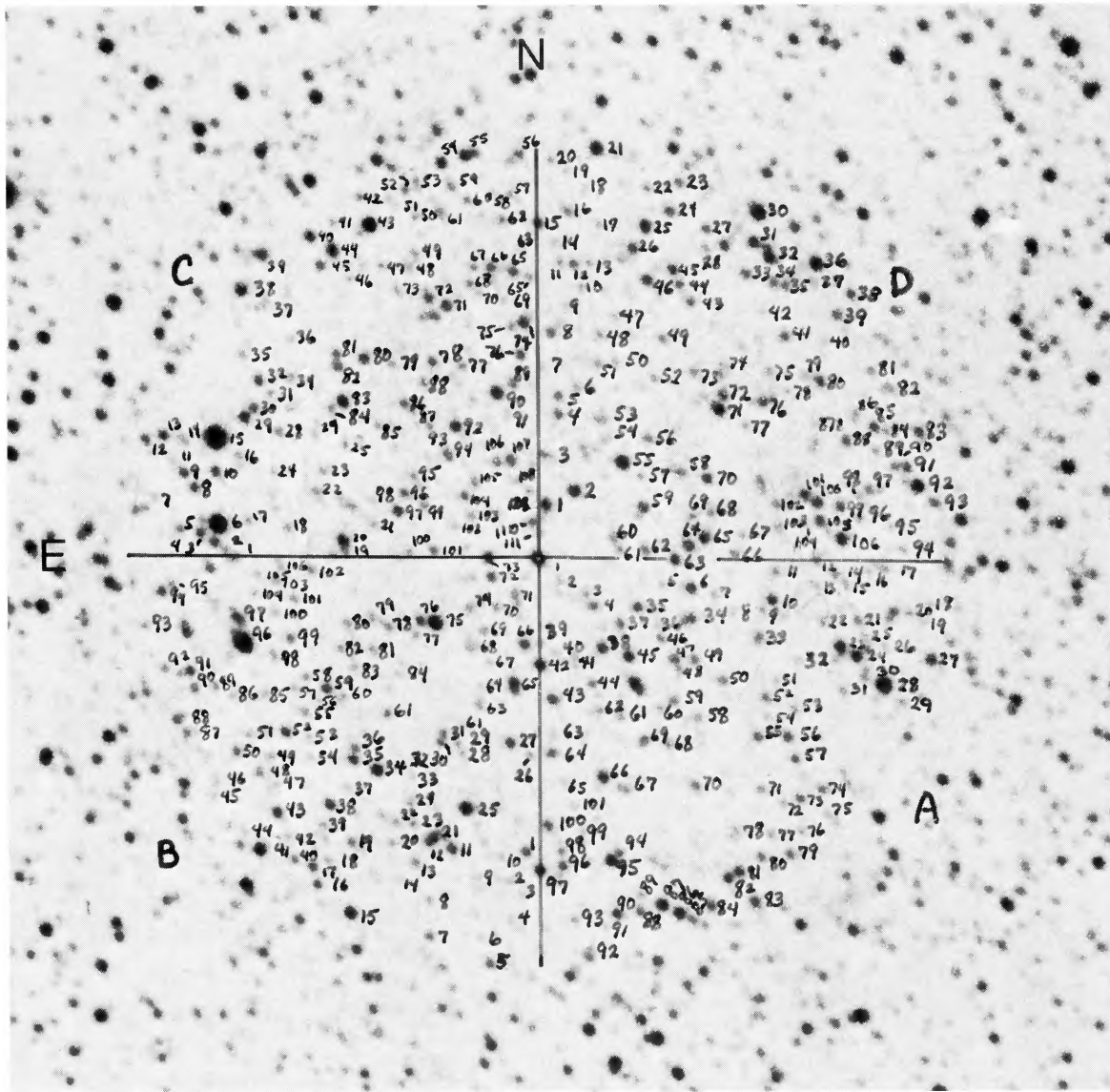


FIG. 4.—An area 4.5' NNW of NGC 2121 with the measured field stars identified

TABLE 4
COLORS AND MAGNITUDES OF FIELD STARS

STAR	V	SE(V)	B-V	SE(B-V)	N	STAR	V	SE(V)	B-V	SE(B-V)	N
A 1	17.74	0.01	0.97	0.12	2	A 82	19.51	0.05	0.27	0.03	2
A 2	20.45	0.05	1.25	0.17	2	A 83	18.54	0.34	1.25	0.33	2
A 3	20.70	0.14	0.75	0.05	2	A 84	18.74	0.22	1.31	0.21	2
A 4	20.07	0.11	0.58	0.04	2	A 85	19.09	0.33	1.21	0.29	2
A 6	19.77	0.06	0.14	0.13	2	A 86	18.82	0.17	0.30	0.02	2
A 7	20.70	--	1.22	--	1	A 87	18.77	0.14	0.45	0.04	2
A 9	20.48	--	1.32	--	1	A 88	20.09	0.01	0.47	0.05	2
A 10	19.62	0.08	0.28	0.02	2	A 89	20.39	0.07	1.00	0.06	2
A 11	20.24	0.00	0.92	0.09	2	A 90	18.66	0.14	1.17	0.08	2
A 12	20.41	0.02	0.60	0.14	2	A 91	21.11	--	0.70	--	1
A 13	21.12	--	0.40	--	1	A 92	19.81	0.14	0.66	0.24	2
A 14	20.67	0.15	0.53	0.03	2	A 93	20.86	--	0.54	--	1
A 15	20.73	0.13	0.88	0.36	2	A 94	19.11	0.02	1.29	0.14	2
A 16	21.23	--	0.62	--	1	A 95	18.89	0.03	0.28	0.09	2
A 17	20.65	--	0.36	--	1	A 96	18.77	0.08	1.26	0.04	2
A 18	20.35	--	1.26	--	1	A 97	18.20	0.11	1.35	0.03	2
A 19	20.89	--	0.82	--	1	A 98	20.00	0.04	1.00	0.12	2
A 20	20.49	0.10	1.00	0.20	2	A 99	20.96	--	0.66	--	1
A 21	19.74	0.07	1.06	0.13	2	A 100	19.79	0.10	0.52	0.12	2
A 22	20.48	0.08	0.93	0.07	2	A 101	20.63	0.11	1.34	0.31	2
A 23	18.10	0.09	0.97	0.04	2	B 1	20.05	0.10	0.41	0.05	2
A 24	18.98	0.06	0.28	0.04	2	B 2	20.60	--	1.05	--	1
A 25	20.68	--	0.76	--	1	B 3	20.92	--	0.92	--	1
A 26	20.82	0.19	1.12	0.40	2	B 5	19.99	0.11	0.49	0.05	2
A 27	18.99	0.47	0.59	0.31	2	B 7	20.11	0.14	0.75	0.21	2
A 28	17.82	0.05	0.25	0.06	2	B 3	20.89	--	0.59	--	1
A 30	19.92	0.29	0.90	0.40	2	B 9	20.50	--	1.38	--	1
A 31	20.49	--	0.83	--	1	B 10	20.82	--	0.94	--	1
A 32	20.65	--	1.12	--	1	B 11	19.80	0.10	0.13	0.03	2
A 33	20.74	0.09	0.09	0.22	2	B 12	19.59	--	-0.27	--	1
A 34	19.92	0.02	0.13	0.06	2	B 13	20.42	0.01	0.53	0.12	2
A 35	20.13	0.24	0.36	0.23	2	B 15	18.82	0.06	0.39	0.06	2
A 37	20.27	0.04	0.44	0.18	2	B 16	20.10	0.01	0.45	0.03	2
A 38	19.76	0.15	0.03	0.21	2	B 17	18.65	0.12	1.37	0.07	2
A 39	21.27	--	0.36	--	1	B 19	19.82	0.04	1.01	0.04	2
A 40	20.74	--	0.96	--	1	B 20	20.61	--	0.86	--	1
A 42	19.25	0.00	0.30	0.07	2	B 21	20.53	--	1.09	--	1
A 43	18.65	0.16	1.16	0.11	2	B 23	20.82	--	0.37	--	1
A 44	20.49	0.25	0.53	0.37	2	B 24	20.93	--	0.35	--	1
A 45	19.15	0.03	0.41	0.15	2	B 25	18.20	0.11	0.69	0.01	2
A 46	19.96	0.07	1.07	0.20	2	B 26	20.58	0.25	0.94	0.30	2
A 47	19.06	0.10	1.16	0.13	2	B 27	18.98	0.11	1.00	0.05	2
A 48	20.09	--	0.78	--	1	B 29	20.82	--	0.52	--	1
A 49	20.30	0.03	0.47	0.12	2	B 30	20.69	--	-0.02	--	1
A 50	20.26	--	0.50	--	1	B 31	20.47	--	0.31	--	1
A 51	20.86	--	0.91	--	1	B 32	20.56	--	1.36	--	1
A 52	20.29	--	0.49	--	1	B 34	18.83	0.17	0.41	0.05	2
A 53	20.19	0.01	1.12	0.11	2	B 35	18.82	0.11	0.93	0.05	2
A 55	20.28	0.13	0.16	0.13	2	B 36	20.12	0.12	0.58	0.04	2
A 56	19.83	0.18	0.43	0.14	2	B 37	20.97	--	0.81	--	1
A 57	20.19	0.11	0.40	0.04	2	B 38	19.46	0.02	0.41	0.04	2
A 58	20.96	--	0.22	--	1	B 39	20.49	--	0.80	--	1
A 59	20.19	0.07	0.75	0.20	2	B 40	19.76	0.00	1.02	0.04	2
A 60	20.74	--	0.85	--	1	B 41	18.55	0.11	0.44	0.02	2
A 61	20.21	0.08	0.97	0.26	2	B 42	21.11	--	0.55	--	1
A 62	20.51	0.12	0.80	0.22	2	B 43	18.44	0.16	1.19	0.07	2
A 64	19.85	0.07	0.66	0.11	2	B 47	20.93	--	0.73	--	1
A 65	20.99	--	0.88	--	1	B 48	20.45	0.23	0.45	0.34	2
A 66	18.93	0.20	0.60	0.10	2	B 49	20.87	--	0.45	--	1
A 67	20.12	0.01	0.41	0.07	2	B 50	19.18	0.15	1.33	0.13	2
A 68	20.29	--	0.68	--	1	B 51	20.77	--	0.76	--	1
A 69	20.50	0.20	0.66	0.36	2	B 52	18.77	0.12	1.26	0.08	2
A 70	20.45	--	0.30	--	1	B 53	20.97	--	0.79	--	1
A 71	20.68	0.26	0.43	0.24	2	B 54	20.87	--	0.92	--	1
A 72	20.61	0.20	0.98	0.35	2	B 55	20.64	0.15	0.53	0.19	2
A 73	20.08	0.01	0.42	0.04	2	B 57	20.97	--	0.49	--	1
A 74	20.45	0.04	0.30	0.00	2	B 58	20.59	0.12	0.74	0.26	2
A 76	20.88	--	0.65	--	1	B 59	19.03	0.11	0.91	0.05	2
A 77	20.56	--	0.88	--	1	B 60	20.81	--	0.54	--	1
A 79	19.73	0.45	0.87	0.49	2	B 61	20.24	--	0.69	--	1
A 80	19.22	0.30	1.27	0.29	2	B 62	20.94	--	0.98	--	1
A 81	19.63	0.03	0.20	0.07	2	B 63	20.33	0.24	0.96	0.36	2

TABLE 4—Continued

STAR	V	SE(V)	B-V	SE(B-V)	N	STAR	V	SE(V)	B-V	SE(B-V)	N
865	19.10	--	0.30	--	1	C42	20.53	0.17	0.80	0.30	2
866	18.46	0.10	1.34	0.04	2	C43	18.29	0.10	0.28	0.04	2
867	20.97	--	0.88	--	1	C44	19.05	0.09	0.37	0.04	2
868	20.56	0.33	0.83	0.48	2	C45	20.14	0.08	0.42	0.01	2
869	20.58	0.04	0.85	0.35	2	C47	20.59	--	0.84	--	1
870	20.71	--	0.65	--	1	C49	20.68	--	0.61	--	1
871	20.48	0.07	0.40	0.17	2	C51	20.56	--	1.06	--	1
872	19.18	0.01	1.16	0.04	2	C52	20.42	0.01	0.45	0.06	2
873	18.74	0.14	1.00	0.09	2	C53	20.47	0.20	0.87	0.33	2
874	20.57	0.20	0.70	0.26	2	C54	18.52	0.12	1.09	0.07	2
875	18.14	0.08	0.34	0.07	2	C55	18.28	0.13	0.96	0.03	2
876	19.87	0.03	0.13	0.13	2	C56	20.13	--	0.31	--	1
877	21.02	--	0.38	--	1	C59	19.94	0.10	0.92	0.02	2
878	20.12	--	0.84	--	1	C60	20.41	0.36	0.75	0.41	2
881	20.24	0.06	1.16	0.16	2	C61	20.79	--	0.03	--	1
882	20.34	0.16	0.96	0.09	2	C62	20.51	0.35	0.62	0.47	2
883	20.28	0.04	1.21	0.03	2	C63	21.09	--	0.93	--	1
887	20.17	0.08	0.62	0.00	2	C64	20.45	--	0.74	--	1
888	19.96	0.02	0.25	0.10	2	C65	18.94	0.21	1.27	0.20	2
889	20.36	--	0.65	--	1	C66	19.16	0.00	1.09	0.01	2
890	20.10	0.16	0.50	0.08	2	C67	20.67	--	0.47	--	1
891	19.74	0.03	0.29	0.04	2	C68	19.84	0.00	1.17	0.11	2
892	20.43	0.13	0.69	0.27	2	C71	18.55	0.09	1.13	0.05	2
893	20.87	--	0.39	--	1	C72	18.76	0.15	1.26	0.13	2
894	18.64	0.17	1.41	0.13	2	C74	19.41	0.02	0.20	0.05	2
895	20.64	0.15	0.71	0.21	2	C75	20.44	--	0.46	--	1
896	16.21	0.03	0.78	0.05	2	C76	19.84	0.03	0.46	0.01	2
897	19.56	--	0.41	--	1	C78	20.14	0.08	0.39	0.10	2
898	20.96	--	0.23	--	1	C79	20.71	0.15	0.55	0.19	2
899	20.10	0.04	0.72	0.07	2	C80	18.59	0.19	1.26	0.11	2
8100	20.80	--	0.81	--	1	C81	20.20	0.05	0.34	0.10	2
8101	20.51	0.06	0.67	0.14	2	C82	19.90	0.07	0.22	0.14	2
8102	20.69	--	0.38	--	1	C83	18.94	0.01	0.38	0.07	2
8103	20.61	--	0.58	--	1	C84	20.28	--	0.67	--	1
8104	20.98	--	0.80	--	1	C86	20.29	0.14	0.34	0.04	2
8105	20.98	--	0.67	--	1	C87	20.19	--	0.79	--	1
8107	19.09	0.08	1.05	0.10	2	C88	20.44	0.09	0.65	0.22	2
C1	19.52	0.07	0.80	0.00	2	C89	20.03	0.08	0.53	0.01	2
C3	19.49	0.07	0.12	0.06	2	C90	17.82	0.07	1.29	0.02	2
C4	19.94	0.19	0.08	0.21	2	C91	20.83	--	0.96	--	1
C5	20.40	0.03	0.35	0.01	2	C92	19.28	0.04	0.35	0.04	2
C6	16.80	0.03	0.54	0.10	2	C93	20.43	--	0.74	--	1
C7	20.90	--	0.77	--	1	C94	19.26	0.17	0.95	0.10	2
C8	18.68	0.14	1.24	0.07	2	C95	20.74	--	0.58	--	1
C9	18.81	0.10	1.18	0.04	2	C96	20.27	0.05	0.48	0.05	2
C10	18.39	0.11	1.50	0.10	2	C97	18.82	0.06	1.02	0.01	2
C12	20.24	0.05	0.25	0.07	2	C99	19.84	0.09	1.19	0.00	2
C13	19.45	0.08	0.51	0.13	2	C100	20.63	--	0.60	--	1
C14	20.73	--	0.18	--	1	C101	20.46	0.10	0.45	0.04	2
C15	15.69	0.01	0.60	0.01	2	C102	20.46	--	1.18	--	1
C16	20.40	0.22	0.92	0.32	2	C103	20.60	0.17	0.71	0.31	2
C17	20.32	--	1.03	--	1	C104	19.31	0.02	1.17	0.05	2
C18	20.11	0.02	1.28	0.10	2	C105	20.18	0.05	0.79	0.10	2
C19	20.76	--	0.59	--	1	C106	20.02	0.09	0.62	0.00	2
C20	19.25	0.02	0.22	0.05	2	C107	19.30	0.05	0.70	0.02	2
C21	20.85	--	0.70	--	1	C108	20.84	--	0.59	--	1
C22	20.58	--	0.53	--	1	C110	20.28	0.07	0.39	0.04	2
C25	20.63	--	0.72	--	1	C112	20.79	--	0.89	--	1
C26	20.98	--	0.79	--	1	D1	18.35	0.12	1.13	0.02	2
C28	20.19	0.15	0.75	0.21	2	D2	18.68	0.08	0.60	0.04	2
C29	19.67	0.40	-0.17	0.42	2	D3	20.07	--	0.81	--	1
C30	19.83	0.10	0.24	0.15	2	D4	19.97	0.03	0.53	0.04	2
C31	20.23	--	0.89	--	1	D5	20.26	0.06	0.60	0.21	2
C32	18.81	0.10	1.25	0.06	2	D6	20.48	--	0.86	--	1
C34	20.61	--	0.56	--	1	D8	20.15	0.17	0.52	0.22	2
C35	20.63	--	0.68	--	1	D12	20.25	0.12	0.48	0.07	2
C36	21.01	--	0.72	--	1	D13	20.69	--	0.79	--	1
C37	20.79	--	0.53	--	1	D14	20.62	0.41	1.18	0.48	2
C38	18.90	0.17	0.44	0.06	2	D15	19.92	0.02	0.27	0.07	2
C39	18.18	0.12	1.22	0.05	2	D16	20.29	0.01	0.69	0.16	2
C40	18.15	0.12	1.47	0.04	2	D17	20.84	--	0.85	--	1
C41	20.83	--	0.67	--	1	D21	18.63	0.13	0.43	0.00	2

TABLE 4—Continued

STAR	V	SE(V)	B-V	SE(B-V)	N	STAR	V	SE(V)	B-V	SE(B-V)	N
D22	20.44	0.00	0.71	0.08	2	D64	18.59	0.12	0.95	0.01	2
D23	19.84	0.06	0.80	0.12	2	D65	19.07	0.05	0.35	0.06	2
D24	19.99	0.05	0.31	0.03	2	D66	20.65	--	0.36	--	1
D25	19.26	0.09	0.17	0.02	2	D68	20.37	0.06	0.70	0.04	2
D26	18.79	0.14	1.21	0.15	2	D69	20.47	--	1.32	--	1
D27	19.93	0.11	0.64	0.15	2	D70	19.93	0.04	0.17	0.06	2
D28	20.69	0.20	0.80	0.29	2	D71	18.64	0.08	0.37	0.03	2
D29	19.77	0.11	0.28	0.11	2	D72	18.82	0.07	1.15	0.09	2
D30	16.89	0.01	1.25	0.08	2	D73	20.47	0.01	0.75	0.17	2
D31	19.15	0.07	0.38	0.00	2	D74	20.39	--	0.69	--	1
D32	18.96	0.02	0.15	0.05	2	D75	20.93	--	0.31	--	1
D33	20.22	--	0.30	--	1	D76	19.79	0.08	0.31	0.08	2
D34	20.15	0.01	0.40	0.16	2	D79	20.63	0.30	0.92	0.42	2
D35	20.03	0.00	0.49	0.10	2	D80	18.89	0.07	1.10	0.05	2
D36	18.40	0.14	0.44	0.00	2	D81	20.41	0.18	0.74	0.28	2
D37	20.81	--	0.52	--	1	D82	20.45	--	0.60	--	1
D38	19.13	0.08	1.24	0.13	2	D83	20.05	0.05	0.11	0.07	2
D39	19.90	0.13	0.40	0.08	2	D84	20.81	--	0.23	--	1
D41	20.08	0.07	0.43	0.08	2	D85	20.05	0.04	0.24	0.08	2
D43	20.22	0.04	0.62	0.08	2	D88	19.97	0.04	0.45	0.01	2
D44	19.79	0.01	0.84	0.05	2	D90	20.31	0.28	0.44	0.36	2
D45	19.86	0.03	0.35	0.03	2	D91	19.06	0.10	0.93	0.01	2
D46	19.63	0.12	0.28	0.08	2	D92	18.14	0.08	0.68	0.07	2
D48	21.13	--	0.22	--	1	D93	19.93	0.00	0.52	0.05	2
D49	20.51	0.07	0.60	0.07	2	D94	20.87	--	0.71	--	1
D50	20.43	--	1.06	--	1	D96	20.88	--	0.37	--	1
D53	20.40	0.19	0.78	0.34	2	D97	20.25	0.01	0.51	0.04	2
D54	20.56	--	0.92	--	1	D98	20.52	--	0.79	--	1
D55	17.09	0.04	1.58	0.09	2	D99	19.94	0.04	0.25	0.04	2
D56	20.26	0.12	0.68	0.20	2	D100	19.39	0.16	0.24	0.08	2
D58	19.78	0.08	0.96	0.19	2	D101	18.39	0.16	1.25	0.09	2
D59	18.61	0.13	1.19	0.06	2	D102	20.55	--	0.41	--	1
D60	20.48	--	0.54	--	1	D103	20.79	--	0.42	--	1
D61	20.56	--	0.64	--	1	D105	18.75	0.07	1.12	0.00	2
D62	20.26	0.14	0.55	0.24	2	D106	17.58	0.04	1.44	0.09	2
D63	19.73	0.02	0.24	0.08	2						

distribution of stars in Figure 5 is quite similar to that in Figure 3, with a conspicuous main sequence rising to $M_v \sim 0$, a large number of stars with $V > 20$ and a spread of color, and a giant region at $V \sim 18.5$, $B-V \sim 1.2$.

In comparing quantitatively the $C-M$ diagrams for NGC 2121 and the field, we must account for the differences in the effective area sampled in each case. In the argument that follows, we use only the outer ring area of NGC 2121, as in the central area the crowding is so severe that we cannot see or count the faint images. In the outer ring we count 804 stars with $V < 20.7$. Of these, 492 were not measured because of the presence of adjoining or partly overlapping images. The field region has an area 1.56 times larger than the outer ring of NGC 2121. There are 434 stars in the field with $V < 20.7$; of these, 172 were not measured because of crowding. Thus we calculate that the total number of field (foreground and LMC background) stars in the NGC 2121 outer ring is 278 and there are 526 cluster stars. In the $C-M$ diagram, however, the contamination depends on the relative crowding and the resulting difference of measuring completeness. Comparing $C-M$ diagrams of NGC 2121 to the field, we find a relative factor of completeness of 0.65. Taking into account the difference in area on the sky,

the final figure is 0.42; that is, 42% of the stars in Figure 5 should have their counterparts contaminating Figure 3 (outer ring).

VII. THE CLUSTER $C-M$ DIAGRAM

In order to illustrate the true morphology of the $C-M$ diagram of the cluster, we have constructed Figure 6 by removing the field stars from the measured $C-M$ diagram. This was done by mapping the field stars' positions to equivalent positions in the cluster diagram and removing 0.42 cluster points nearest to the position of each field star. Thus Figure 6 represents a statistically corrected $C-M$ diagram for cluster stars only. It shows a substantial number of main sequence stars reaching to $V \approx 19.7$ with a scattering of brighter stars, which probably include some uncorrected-for field stars, as well as some evolved giants. The main sequence stars show a broad range in color, due to the growth of photometric errors at these magnitudes, discussed in § III. Although the mean color at the faint limit seems too red, ($\bar{B}-V$ for $V > 19.7 = +0.73$), we believe that this represents a systematic error in color due to crowding and that most, if not all, of these stars are probably blue, with $B-V \approx +0.4$, as expected for the reddened LMC main sequence.

The giant stars show a well-defined array, consisting

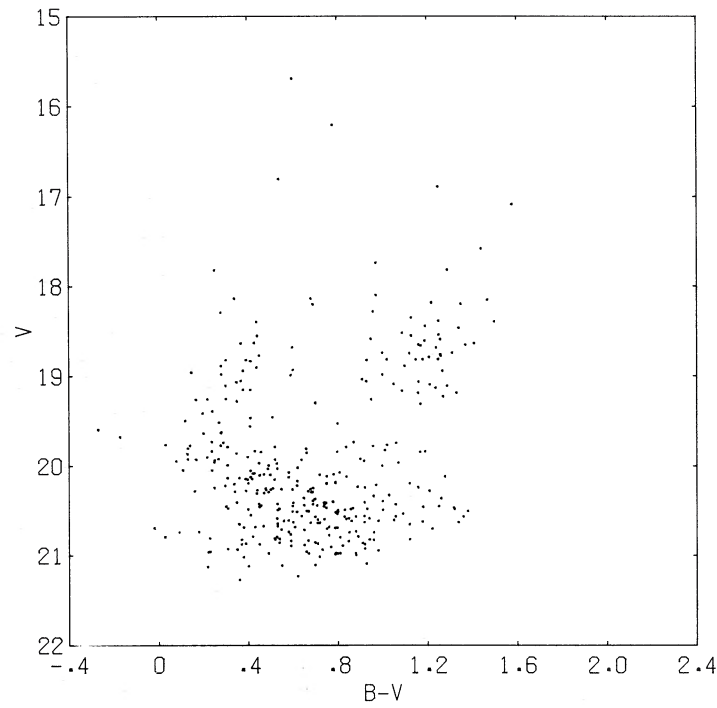


FIG. 5.—The $C\text{-}M$ diagram for the field stars identified in Fig. 4

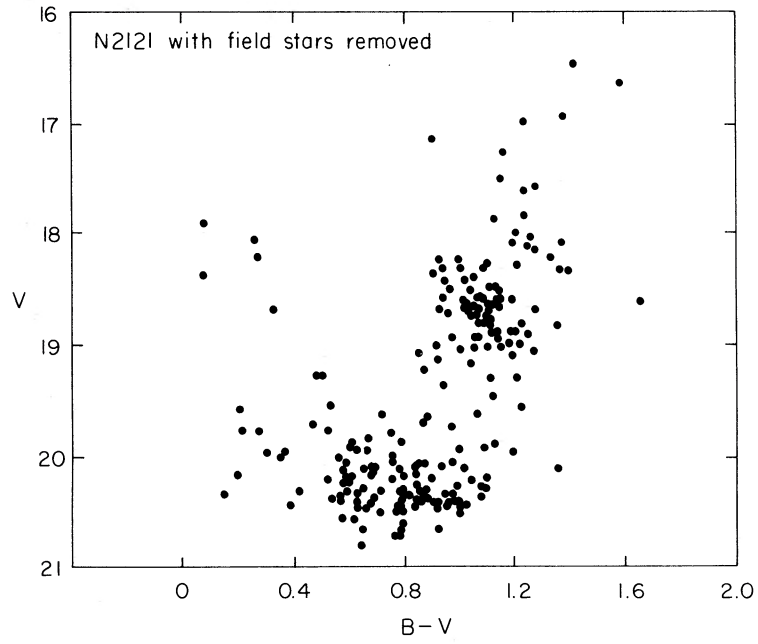


FIG. 6.—A “cleaned” $C\text{-}M$ diagram for the outer ring of NGC 2121, with the field stars removed. See Fig. 10 for inner ring CMD only.

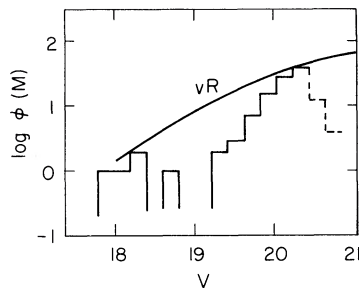


FIG. 7.—The luminosity function for the main sequence stars, corrected for field stars and compared to the van Rhijn function, normalized at $V = 20.3$. The dotted line indicates incompleteness of sampling at the faint end.

of a “clump” with its center at $B-V = 1.1$ and $V = 18.7$, with an extension of brighter and cooler stars to $B-V = 1.5$ and $V = 16.6$. Adjusting for reddening and for the distance of the LMC, the clump’s location becomes $(B-V)_0 = 0.9$, $M_V = -0.4$. The red tip of the giant branch is at $(B-V)_0 = +1.3$, $M_V = -2.5$. There are no anomalous giants of the type discovered in several other Magellanic Cloud clusters (Hodge 1981b; Olszewski 1982).

VIII. THE AGE OF NGC 2121

NGC 2121 is clearly not an example of a true, old globular cluster. To determine its age, we have used three approaches. The first follows the standard procedure of fitting the main sequence tip to evolutionary models, adopting a value of Z from spectroscopic evidence. We interpret the top of the unevolved main sequence to be the position where there is a sudden decrease in the luminosity function (Fig. 7), which occurs at $V = 20.0 \pm 0.4$, which is $M_V = 0.9 \pm 0.5$. The uncertainty in this quantity reflects both the ± 0.2 mag uncertainty in the LMC distance scale (Sandage and Tammann 1974; de Vaucouleurs 1978) and the ± 0.3 mag due to the uncertain reddening. We adopt for the moment a value of $[Z/Z_\odot] = -1$, noting that the age is not very sensitive to Z in the Brunish (1982) models that we use as part of the composite of various theoretical results given in Hodge (1983). From these data we derive an age of $4 \pm 2 \times 10^8$ years. This is smaller than the age of 7×10^8 years derived previously and quoted in that reference, due to this paper’s larger value for the adopted reddening (the previous paper assumed the mean LMC reddening of $E_{B-V} = 0.05$).

A second value for the age is far more tentative, coming from the brightness of the brightest evolved blue giants, which are sparse in NGC 2121 and contaminated by field stars so that statistical corrections are tentative. We adopt $V_{BS} = 19.3 \pm 0.5$, which leads to an age estimate, again using Figure 1 in Hodge (1983), of 4×10^8 yr, with an uncertainty of a factor of about 2.

Our third estimate of the age is more elaborate, requiring calculation of a new set of evolutionary models and the development of new age criteria from the resulting properties of the model giants. Details of the

TABLE 5
CHARACTERISTICS OF THE EVOLUTIONARY MODELS

Mass Range (M_\odot)	Z	Mixing Length	$\sim [Fe/H]$	n	N2121 age (10^9 yr)
2.50–3.25	0.01	1.36	-0.2	4	0.26
2.15–3.20	0.005	1.15	-0.5	7	0.30
2.10–3.10	0.003	1.0	-0.7	9	0.34
2.05–2.90	0.0016	1.0	-1.0	7	0.38
2.10–2.80	0.001	1.0	-1.2	5	0.40

model calculations are given elsewhere (Flower 1983). Table 5 summarizes the properties of those models used here. For all models we used $Y = 0.25$ and a ratio of mixing length to pressure scale height of 1.5. We adopt a parameter, $M_{V,LO}$ as an age criterion. It is taken at the evolutionary phase where model luminosities begin to increase after the rapid luminosity drop occurring just after core helium ignition. We refer to this phase as LO for *Loop Onset*. The rationale for using LO as an age indicator is that any star fainter than the corresponding M_V has to be older, i.e., less massive. We are actually locating the most recently formed red giant. Evolution here is on a nuclear time scale, so we expect a clump of giants on the C - M diagram. It is important to note that because the models have just started helium burning, the ages at LO are virtually independent of the helium burning reaction rates. Since most codes use the same hydrogen burning rates, LO ages should be the same, to within $\sim \pm 5\%$, for all codes. We used $B.C. = -0.22$ to convert model M_{bol} to M_V ; the uncertainty is $\sim \pm 0.1$ mag.

We show in Figure 8 the results in terms of the values of $M_{V,LO}$ as a function of age for the different models. Figure 9 gives a sample comparison of two tracks that illustrates the effect on $M_{V,LO}$ of different values of Z ; clearly, this quantity, at least in this mass

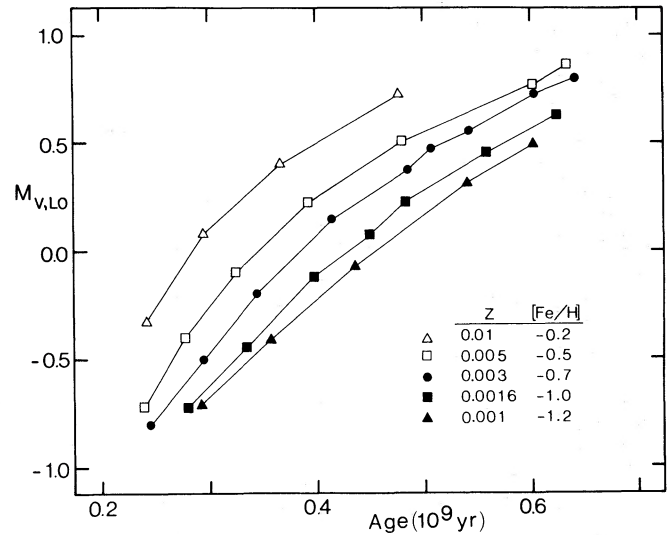


FIG. 8.—Absolute magnitudes of the loop onset as a function of age for different compositions.

range, is not very sensitive to Z . Also Figure 9 shows the effect of Z on the color of the giants, as will be discussed below.

Figure 10 gives an example of a direct comparison between the models and the stellar measures. For this example, we used the $Z = 0.005$ track and the stars with $V \lesssim 18.8$ measured in the inner part of NGC 2121. Conversion to the theoretical plane was effected using the temperature scales of Böhm-Vitense (1981) and Flower (1976), which are virtually identical in this region. Clearly the data and theory agree quite well.

Comparing Figures 8 and 6 leads to a series of age estimates for the five models, which primarily differ in their values of Z . Table 5 (last column) gives the resulting ages. Clearly, regardless of the value of Z , we derive an age of $3-4 \times 10^8$ years for the cluster. As mentioned above, we believe that a value for $[Fe/H] \sim -1.0$ is probably correct, and if this can be taken as equivalent to $Z = 0.0016$, then the age is found to be 3.8×10^8 yr. The uncertainties in this value can be estimated from the information in Table 6. Thus, the total uncertainty in the derived age is probably on the order of $\pm 1.0 \times 10^8$ yr. (The above uncertainties do not include observational errors or uncertainties in the LMC distance or the reddening.)

Finally, we can estimate the age from the integrated $U-B$ color and Hodge's (1983) age-color calibration. This much cruder method gives an age of $2-3 \times 10^8$ yr, but because of the uncertainties in the reddening

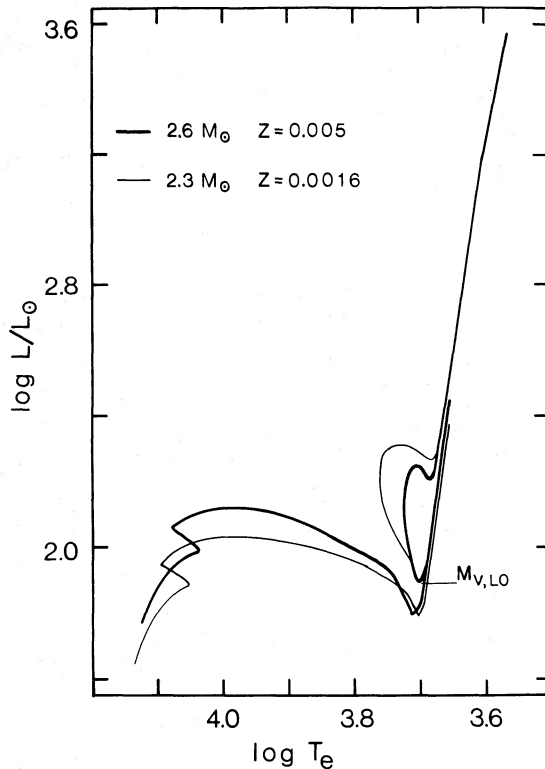


FIG. 9.—A sample comparison of two evolutionary tracks, showing the effect of different values of Z .

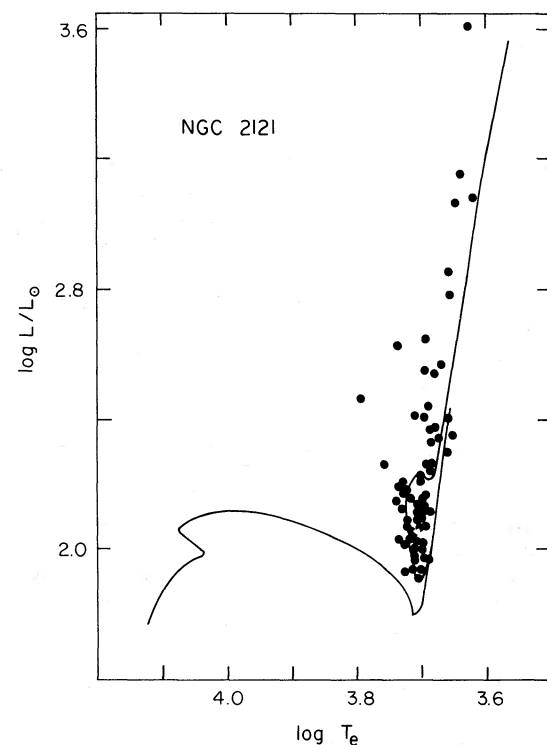


FIG. 10.—A comparison of the positions of the observed stars in NGC 2121 (inner region only) with one of the model tracks (that shown is for $Z = 0.005$).

and the double valued nature of the calibration relation, this is a very weak determination.

The agreement in the derived ages for NGC 2121 from the four different methods indicates that NGC 2121 is a relatively young cluster. We adopt an age of $4.0 \pm 2.0 \times 10^8$ years as the best value from the $C-M$ diagram. This clearly disagrees with the early ideas that NGC 2121 is a true globular cluster. It also disagrees with Mould and Aaronson's (1982) suggestion from its carbon star that its age is less than but on the order of 4×10^9 yr. However, the carbon-star age criterion apparently suffers from systematically overestimating ages for clusters with ages less than 10^{10} years, as shown for nine Magellanic Cloud clusters that have $C-M$ diagram ages (Hodge 1983). Similarly, Rabin's (1982) age estimate of $\sim 5-10 \times 10^9$ yr seems too large. This

TABLE 6
UNCERTAINTIES IN THE MODEL PARAMETERS
AND AGE ESTIMATES

Parameter	Δ	$\Delta t \times 10^8$ yr
B.C.	± 0.1	± 0.2
V	± 0.1	± 0.2
Y	± 0.05	± 0.8
Fe/H	± 0.3	± 0.6
Code	est.	± 0.2

latter point is a particularly bothersome and unsolved problem, as his spectrum (his Fig. 2) of NGC 2121 is very similar to those of bona fide old clusters.

IX. THE CHEMICAL COMPOSITION OF NGC 2121

With the age established, it is now possible to use the *C-M* diagram to estimate the heavy-element abundance of the cluster. Of course, we cannot do more than judge this on the basis of the collective effects of heavy elements on the models of the evolved giants, without being able to distinguish the relative importance of various groups of elements (e.g., CNO, metals, etc.). We can only derive a preferred value for Z , assuming the elements to be distributed among themselves in the standard way.

We have approached the problem in two ways. First, we have used the semiempirical relationship, based on a composite of various theoretical models (e.g., Ciardullo and Demarque 1977; Kinahan and Härm 1975; Gustafson, Bell, and Hejlesen 1977; Flower *et al.* 1980) that was proposed by Hodge (1982). This gives a value of $Z = 0.0006 \pm 0.0004$, where the uncertainty refers to the possible errors in the determination of $(B-V)_1$ and in the reddening.

Our second approach uses the models calculated for this paper (Fig. 8) and the age determined above, noting however, that our third age determination above was based on the same graph and an assumed value of Z , so it cannot be included here. Using 4.0 ± 2.0

$\times 10^8$ years as an age, we find a value for Z of 0.001, with an upper limit of 0.005 and a lower limit that is beyond the range of Figure 8.

Combining these results by taking a straight mean gives us $Z = 0.0008$ or $[Fe/H] \approx -1.3$, with an uncertainty in $[Fe/H]$ of about ± 0.4 . This value is in agreement with the spectroscopic result of Rabin (1982) and consistent with that of Cohen (1982). Considering all three sources and giving the individual stellar spectra double weight, we conclude that for NGC 2121, $[Fe/H] = -1.1 \pm 0.2$.

In conclusion, we find that the color-magnitude diagram of the luminous, large, red LMC cluster NGC 2121 indicates that it is of intermediate age, with $t \approx 4 \times 10^8$ years. Its heavy-element abundance is low, with $[Fe/H] \approx -1.1$, and it is thus an example of a "young globular cluster," with the dimensions and abundances of a normal globular cluster, but of young age. A deeper *C-M* diagram, obtained for example with a CCD, could help to increase the accuracy of these parameters.

We are indebted to the Cerro Tololo Inter-American and the Las Campanas Observatories for making their observing facilities available to us, to N. Suntzeff for helpful discussions, and to the National Science Foundation, which partially supported this research through grant 81-02952 to P. W. H.

REFERENCES

- Blanco, V. M. 1982, *Pub. A.S.P.*, **94**, 201.
- Böhm-Vitense, E. 1981, *Ann. Rev. Astr. Ap.*, **19**, 295.
- Böhm-Vitense, E., Borutzki, S., and Harris, H. 1982, preprint.
- Brunish, W. 1982, *Ap. J. Suppl.*, **49**, 447.
- Ciardullo, R., and Demarque, P. 1977, *Trans. Astr. Obs. Yale Univ.*, Vol. 33.
- Cohen, J. G. 1982, *Ap. J.*, **258**, 143.
- Daniziger, I. J. 1973, *Ap. J.*, **181**, 641.
- Demers, S. 1973, *A.J.*, **78**, 461.
- de Vaucouleurs, G. 1978, *Ap. J.*, **223**, 351.
- Flower, P. 1976, Ph.D. thesis, University of Washington.
- . 1982, *Pub. A.S.P.*, **94**, 894.
- . 1983, *Ap. J.*, in press.
- Flower, P., Geisler, D., Hodge, P., and Olszewski, E. 1980, *Ap. J.*, **235**, 769.
- Frenk, C., and Fall, S. M. 1982, *M.N.R.A.S.*, in press.
- Gascoigne, S., and Kron, G. 1952, *Pub. A.S.P.*, **64**, 196.
- Geisler, D., and Hodge, P. 1980, *Ap. J.*, **242**, 66.
- Gustafson, B., Bell, R., and Hejlesen, P. 1977, *Ap. J.*, **216**, L7.
- Hartwick, F. D. A., and Hesser, J. E. 1977, *Ap. J. Suppl.*, **33**, 361.
- Hesser, J., Hartwick, F. D., and Ugarte, P. 1976, *Ap. J. Suppl.*, **32**, 283.
- Hodge, P. 1960, *Ap. J.*, **131**, 351.
- . 1981a, in *Astrophysical Parameters for Globular Clusters*, ed. A. Philip and D. Hayes (Schenectady: Davis Press).
- . 1981b, *J. Ap. Astr.*, **2**, 161.
- . 1982, *Ap. J.*, **256**, 447.
- . 1983, *Ap. J.*, **264**, 470.
- Hodge, P., and Wright, F. 1963, *Ap. J.*, **138**, 366.
- . 1966, *A.J.*, **71**, 131.
- Kinahan, B., and Härm, R. 1975, *Ap. J.*, **200**, 330.
- Lloyd Evans, T. 1980, *M.N.R.A.S.*, **193**, 87.
- Lucke, P. 1974, *Ap. J. Suppl.*, **28**, 73.
- Mould, J., and Aaronson, M. 1982, *Ap. J.*, **263**, 629.
- Olszewski, E. 1982, Ph.D. thesis, University of Washington.
- Pickering, E. C. 1891, *Ann. Harvard Obs.*, **27**, 14.
- Racine, R. 1969, *Ap. J.*, **74**, 1073.
- Rabin, D. 1982, *Ap. J.*, **261**, 85.
- Sandage, A., and Tammann, G. 1974, *Ap. J.*, **190**, 525.
- Searle, L., Wilkinson, A., and Bagnuolo, W. 1980, *Ap. J.*, **239**, 803.
- Tody, D. 1980, in *S.P.I.E. Symp. Applications of Digital Image Processing to Astronomy*, ed. D. A. Elliott, p. 121.
- van den Bergh, S. 1981, *Astr. Ap.*, **46**, 79.

PHILLIP J. FLOWER: Department of Physics and Astronomy, Clemson University, Clemson, SC 29631

DOUGLAS P. GEISLER and PAUL W. HODGE: Astronomy Department FM-20, University of Washington, Seattle, WA 98195

EDWARD W. OLSZEWSKI: Dominion Astrophysical Observatory, 5071 W. Saanich Road, Victoria, B.C. V8X 4M6, Canada

ROBERT A. SCHOMMER: Department of Physics and Astronomy, Rutgers University, P.O. Box 849, Serin Phys. Lab., Piscataway, NJ 08844